CHAPTER 2

Generation–Recombination Noise in Semiconductors

V. Mitin
Department of Electrical and Computer Engineering, Wayne State University, Detroit, Michigan, USA

L. Reggiani
INFM–National Nanotechnology Laboratory, Dipartimento di Ingegneria dell' Innovazione, Università di Lecce, Via Arnesano s/n, Lecce, Italy

L. Varani
Centre d'Electronique et de Micro-optoélectronique de Montpellier (CNRS UMR 5507), Université Montpellier II, Montpellier Cedex 5, France

CONTENTS

ISBN: 1-58883-000-4 / $35.00

Noise and Fluctuations Control in Electronic Devices,
Edited by A. Balandin

1. INTRODUCTION

Generation–recombination (GR) noise is due to fluctuations in the number of free carriers inside of a two-terminal sample associated with random transitions of charge carriers between states in different energy bands. Accordingly, it represents a typical noise source in semiconductor materials where carrier concentration can vary over many orders of magnitude. Typical examples of transitions are between conduction band and localized levels in the energy gap, conduction and valence bands, etc. Therefore, GR noise is inherently due to fluctuations of carrier number, usually keeping charge neutrality of the total sample.

The first experimental evidence of GR noise in semiconductors dates the 1951, and its physical interpretation (together with the introduction of the GR name) was given a few years later [1]. Since then, many experiments were performed on a variety of semiconductor materials and devices and detailed theories were developed. For widely used reviews and books summarizing the present knowledge we address the reader to Refs. [2–9].

The essence of GR noise can be illustrated by considering the simple system provided by a macroscopic semiconducting resistor with resistance R in which the instantaneous number of free electrons $N(t)$, taken as majority carriers, fluctuates between two levels, that is, the conduction band and the donor impurities. Within a relaxation time approximation, GR noise can be related to the resistance R (conductance $G = 1/R$) fluctuations with spectral densities given by

$$\frac{S_R(\omega)}{R^2} = \frac{S_G(\omega)}{G^2} = \frac{S_N(\omega)}{N_0^2} = \frac{\overline{\delta N^2}}{N_0^2}\frac{4\tau_N}{1+(\omega\tau_N)^2} \tag{1}$$

with $S_R(\omega), S_G(\omega), S_N(\omega)$ the spectral density of resistance, conductance, and carrier number, respectively, $\omega = 2\pi f$ the circular frequency, $\overline{\delta N^2}$ the variance of carrier number fluctuations, $N_0 = \overline{N}$ the average number of free carriers with bar denoting ensemble or time average (ergodicity is usually assumed to hold), and τ_N the carrier lifetime.

The spectrum of the fluctuations in Eq. (1) is of Lorentzian type with two parameters, that is, the relative variance of number fluctuations and the lifetime of charge carriers, to be determined. The above spectrum generally refers to thermal equilibrium conditions. As such, when measuring current or voltage fluctuations it can be detected only as excess noise, defined as the electron noise beyond that of thermal equilibrium (Nyquist noise) in the presence of an external bias (voltage V or current I). By assuming that the external bias does not modify the noise sources, and treating the noise sources as independent, a suitable way to detect experimentally GR noise is to analyze an excess noise spectrum in terms of a phenomenological expression for the current spectral density, $S_I(\omega)$, which includes also Nyquist [10] and $1/f$ (or flicker) [2] unavoidable contributions as

$$S_I(\omega) = 4K_BT\,\mathrm{Re}[Y(\omega)] + I^2\frac{S_N(\omega)}{N_0^2} + I^2\frac{2\pi C}{\omega} \tag{2}$$

with K_B the Boltzmann constant, T the bath temperature, $\mathrm{Re}[Y(\omega)]$ the real part of the small signal admittance, and C a numerical parameter giving the strength of the $1/f$ contribution. (Quantum corrections are here neglected; that is, the $\hbar\omega/(K_BT) \ll 1$ condition is assumed henceforth.)

The analogous expression for the voltage spectral density $S_V(\omega)$ is written

$$S_V(\omega) = 4K_BT\,\mathrm{Re}[Z(\omega)] + V^2\frac{S_N(\omega)}{N_0^2} + V^2\frac{2\pi C}{\omega} \tag{3}$$

with $\mathrm{Re}[Z(\omega)]$ the real part of the small signal impedance. We note that the relation

$$Y(\omega)Z(\omega) = 1 \tag{4}$$

is always satisfied.

The typical cutoff frequencies are (i) over the THz region for thermal noise, (ii) below the GHz region for GR noise, and (iii) below the MHz region for $1/f$ noise. As a consequence, the noise spectrum can usually be resolved in frequency thus providing the GR parameters with sufficient accuracy through the determination of the plateau and the corner frequency, as depicted in Figure 1 where the noise spectrum of n-Si [11, 12] is shown to be fitted on the basis of Eq. (2). We note that to better evidence GR from $1/f$ noise it is sometimes convenient to plot on a log-log scale the product $\omega S_I(\omega)$ vs. ω so that the presence of GR noise emerges in forms of peaks over a $1/f$ spectrum [13].

The above identification of GR noise is in general complicated by several phenomena which makes the excess noise spectrum quite far from the simple type proposed above, as summarized in the following main points.

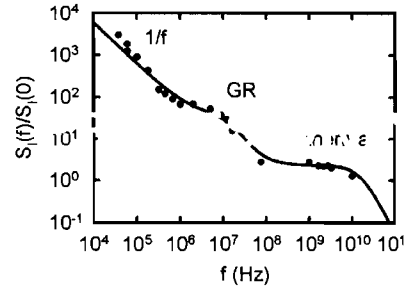

Figure 1. Schematic of a current spectral density evidencing $1/f$, GR, and thermal noise sources at increasing frequencies. Full circles are experiments on n-Si after Ref. [12]. The curve is a fitting using Eq. (2) in the form $S_I(\omega) = A/[1+(\omega\tau_m)^2] + B/[1+(\omega\tau_N)^2] + 2\pi C/\omega$, with $A = 2.3$, $B = 3.0$, $C = 6.0 \times 10^7$ Hz, $\tau_m = 10$ ps, $\tau_N = 10$ ns.

(1) The complexity of the bands and the associated energy levels introduce many possibilities of different and/or simultaneous GR processes.

(2) The applied bias can modify the noise sources (e.g., hot-carrier effects, Poole–Frenkel effect [14, 15], etc.) by also coupling the sources with each other, thus introducing cross-correlation contributions. The applied bias can also originate new GR mechanisms not present at thermal equilibrium or low bias.

(3) The nonuniformity of the local electric field and/or of the structure, typical of electronic devices, requires one to couple self-consistently the transport with the local electric field.

The objective of this chapter is to review GR noise in semiconductors in the light of the points mentioned above. The possibility of obtaining information by GR noise not otherwise available from other measurements and to use it as a tool of reliability will be considered. Finally, we note that an analogous kind of excess noise due to fluctuations of the microscopic scattering cross section among different possible states (usually called mobility fluctuations) can be more or less independently present. This fluctuation of the scattering cross section is clearly noticed in (dirty) metals where GR noise is absent in view of the absence of fluctuations in the number of free carriers [16–18].

2. THEORETICAL APPROACHES

The theoretical approaches to GR noise can be grouped into three main groups, which also reflect the historical development of the subject, namely: (i) the master equation for number fluctuations between two or more levels, here called the standard theory; (ii) the Langevin equation within the hydrodynamic formalism, in the absence and in the presence of carrier transport (in the latter case it constitutes a tenet for the development of the impedance field method and its successive implementations); and (iii) the Boltzmann–Langevin equation and the Monte Carlo method within a kinetic level. In (ii) and (iii) the Poisson equation is usually coupled self-consistently to account for space nonhomogeneous conditions.

Below we first survey the master equation approach for the simple two-level model. On this basis, we provide a classification scheme of the most significant mechanisms with respect to the band structure in real and momentum spaces of the system under study. Then, the other lines of approach, mostly based on a Langevin scheme, will be considered.

2.1. The Standard Theory

For the simple GR two-level system, the standard theory assumes the existence of a generation probability per unit time $g(N)$ and a recombination probability per unit time $r(N)$ which describe the transition from the impurity level to the conduction band and the reverse process, respectively, within a master equation approach [19]. It is further assumed that both rates g and r depend explicitly only on the instantaneous number of carriers in the conducting band, $N(t)$. In general g is a decreasing function of N while r is an increasing function of N, and these functions are modeled according with the physical process under investigation. In steady state conditions, the balance between generation and recombination for $g_0 = g(N_0)$ and $r_0 = r(N_0)$ gives

$$g_0 = r_0 \tag{5}$$

and the probability $P(N)$ of finding N electrons in the conduction band at time t is well approximated by a normal law for $N(t)$ close to the steady state value N_0 as

$$P(N) = P(N_0) \exp\left[-\frac{(N - N_0)^2}{2\overline{\delta N^2}}\right] \tag{6}$$

By defining the generation rate as $1/\tau_g = -g_0'$ and the recombination rate as $1/\tau_r = r_0'$, with $g_0' = dg/dN_{N=N_0}$ and $r_0' = dr/dN_{N=N_0}$, the above expressions lead to

$$\tau_N = \frac{1}{r_0' - g_0'} \tag{7}$$

$$\overline{\delta N^2} = \frac{g_0}{r_0' - g_0'} = g_0 \tau_N \tag{8}$$

$$S_N(\omega) = 4 g_0 \tau_N^2 \frac{1}{1 + (\omega \tau_N)^2} \tag{9}$$

which, in the time domain, imply a correlation function for number fluctuations, $C_N(t)$, of standard exponential form with a lifetime, τ_N:

$$C_N(t) = \overline{\delta N^2} \exp(-t/\tau_N) \tag{10}$$

The quantities g, r, τ_g, τ_r, as well as τ_N and $\overline{\delta N^2}$ can be calculated by a physical modeling of the generation and recombination processes. In another approach, the lifetime and the variance can be fitted to experiments and their microscopic interpretation can be given in terms of capture cross sections and band structure. In the following section we provide a classification of the relevant microscopic mechanisms of GR related to semiconductors.

2.2. Classification Scheme

Generation–recombination processes are specialized below within a real space representation of the band structure and a momentum representation of the band structure.

2.2.1. *Real Space Representation*

With reference to a real space representation of the band structure the GR processes can be specialized as follows. The order of presentation reflects the importance of different mechanisms at increasing values of the temperature [3,4].

Extrinsic We consider an n-type semiconductor with N_D number of donors, $N_A < N_D$ number of acceptors, and N_0 average number of electrons in the conduction band, as illustrated in Figure 2. Then, according to the law of mass action we can write

$$g(N_0) = \gamma(N_D - N_A - N_0) \tag{11}$$

$$r(N_0) = \rho N_0(N_0 + N_A) \tag{12}$$

$$\tau_N = \frac{1}{\rho(2N_0 - N_A) + \gamma} \tag{13}$$

$$\overline{\delta N^2} = N_0 \times \left[\frac{(N_0+N_A)(N_D-N_A-N_0)}{N_0N_D+(N_0+N_A)(N_D-N_A-N_0)}\right] \tag{14}$$

with γ and ρ parameters (with frequency dimension) representing the strength of the generation and recombination processes, respectively. Typical values of γ for the fast processes are in the range of 10^6–10^9 s^{-1}. We note that the equation for the variance has been factorized in the product of N_0 with a term enclosed between squared brackets representing the usual Fano factor $\overline{\delta N^2}/N_0$ to emphasize the deviation of $\overline{\delta N^2}$ from the full Poissonian value N_0 (i.e., corresponding to a unity value of the Fano factor) and determined by the correlation between different elemental processes. Indeed, sub-Poissonian statistics, typical of a repulsive correlation, are evidenced here and in most of the cases considered below.

For transitions between acceptors and the valence band when $N_A > N_D$, analogous results are easily obtained by interchanging N_D with N_A, and N_0 with the average number of holes in the valence band P_0. The previous

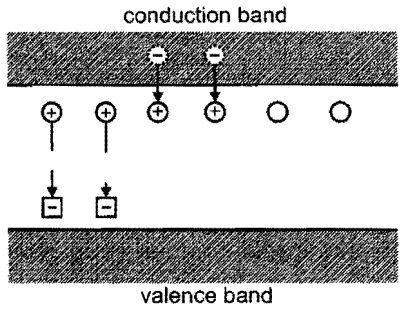

Figure 2. Energy band diagram and electron transitions involved in the fluctuations of conduction electrons in an n-type extrinsic semiconductor with N_D the number of donors, $N_A < N_D$ the number of acceptors, N the number of electrons in the conduction band, and $P = 0$ the number of holes in the valence band. Arrows indicate the direction of transition of an electron to the trapping center.

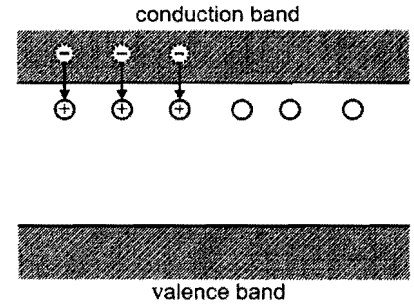

Figure 3. Energy band diagram and electron transitions involved in the fluctuations of conduction electrons in an n-type strongly extrinsic semiconductor with N_D the number of donors, N the number of electrons in the conduction band, and $P = 0$ the number of holes in the valence band. Arrows indicate the direction of transition of an electron.

expressions contain the two limiting cases $N_0 \ll N_A$ and $N_0 \gg N_A$ corresponding to the conditions of very low and high temperature, respectively.

Strongly Extrinsic Let us consider in detail the case in which $N_D \gg N_A$ and holes as minority carriers can be neglected, as illustrated in Figure 3. Then it is

$$g(N_0) = \gamma(N_D - N_0) \tag{15}$$

$$r(N_0) = \rho N_0^2 \tag{16}$$

$$\tau_N = \frac{1}{2\rho N_0 + \gamma} \tag{17}$$

$$\overline{\delta N^2} = N_0 \times \left[\frac{N_D - N_0}{2N_D - N_0}\right] \tag{18}$$

A microscopic interpretation of the generation–recombination process in this case proceeds as follows. At thermal equilibrium, here emphasized by the subscript eq in the relevant variables, the generation and recombination rates are interrelated by the balance equation

$$\gamma_{eq}(1 - u_{eq}) = \rho_{eq} N_D u_{eq}^2 \tag{19}$$

with $u_{eq} = N_0/N_D$ the fraction of ionized carriers, $B_{eq} = \rho_{eq}N_D/n_D$ the recombination rate times the unit volume, which is the suitable parameter to be determined from experiments, and n_D the donor concentration. The recombination rate is related to the energy dependent capture cross section, $\sigma(\epsilon)$, by the standard relation

$$\rho_{eq} = n_D\langle v_0(\epsilon)\rangle \frac{\langle v_0^2(\epsilon)\sigma(\epsilon)\rangle}{\langle v_0^2(\epsilon)\rangle} = n_D\langle v_0\rangle\langle\sigma\rangle \tag{20}$$

where the averages are taken over the forward velocity of the equilibrium energy distribution function and, within a carrier effective mass model m^*, it is $\langle v_0\rangle = \sqrt{8K_BT/(\pi m^*)}$. Typical values for the largest capture cross section at 4 K are of the order of [5] 10^{-10} cm^2. The generation rate can be independently calculated within a

quantum mechanical approach. From the balance equation and the u_{eq} given by statistics, γ_{eq} is related to B_{eq} by

$$\gamma_{eq} = B_{eq} N_N (m^* T)^{3/2} g_D \exp[-(E_c - \epsilon_D)/K_B T)] \quad (21)$$

with $N_N = 4.83 \times 10^{21}$ m^{-3} K$^{-3/2}$ a universal constant factor, g_D the spin degeneracy factor of the order of unity, and ϵ_D the energy of the impurity level as measured from the bottom of the conducting band E_c. Note that in this framework the lifetime takes the usual form

$$\tau_N = 1/(2\langle v_0\rangle\langle\sigma\rangle n_D N_0 + \langle v_0\rangle\langle\sigma\rangle N_N (m^* T)^{3/2} g_D \times \exp[-(E_c - \epsilon_D)/K_B T]) \quad (22)$$

The above relationship is used to construct the Arrehnius plot of $\tau_N T^2$ versus $1/T$ which, for a temperature independent cross section, exhibits a slope proportional to the activation energy of the trap at high temperatures and a slope proportional to the carrier concentration $n = n_D N_0$ at low temperatures, as illustrated in Figure 4. We recall that among the different mechanisms of generation–recombination an important role is played by the nonradiative capture via phonon emission [5].

The presence of an applied electric field E high enough to produce hot carrier effects influences the generation–recombination process by (i) changing the shape of the impurity potential (Poole–Frenkel effect) and thus the generation rate, and (ii) changing the equilibrium distribution function and thus the recombination rate via the average value of the capture cross section. Within a phenomenological approach, the field dependent generation rate takes the form [20]

$$\gamma^{PF}(E) = \gamma_{eq} \exp(a\beta E^{1/2}/K_B T) \quad (23)$$

with $a = 0.5$–1 a numerical parameter accounting for geometrical effects and $\beta = (e^3/\pi\epsilon_0\epsilon_r)^{1/2}$ the Poole–Frenkel constant [5] with e the unit charge, ϵ_r the relative static dielectric constant of the material, and ϵ_0 the vacuum permittivity. Hot carrier effects can be accounted for by using an electron temperature model for the carrier distribution function.

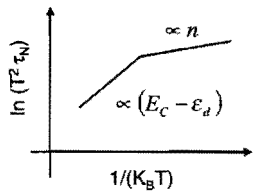

Figure 4. Schematic of the Arrenhius plot of $\tau_N T^2$ versus $1/(K_B T)$ exhibiting the characteristic slopes associated with the carrier lifetime given in Eq. (22).

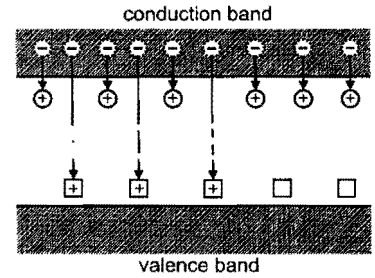

Figure 5. Energy band diagram and electron transitions involved in the fluctuations of conduction electrons in an n-type extrinsic semiconductor with N_D the number of donors fully ionized, N_t the number of traps which are neutral when occupied, N the number of electrons in the conduction band, and $P = 0$ the number of holes in the valence band. Arrows indicate the direction of transition of an electron.

Extrinsic With Electron Traps Let us consider the case with N_D fully ionized donors, N_T partially ionized donor traps, and negligible minority carriers in the valence band. The traps are assumed to be neutral when occupied, as illustrated in Figure 5. Thus

$$g(N_0) = \gamma(N_D + N_T - N_0) \quad (24)$$

$$r(N_0) = \rho N_0 (N_0 - N_D) \quad (25)$$

$$\tau_N = \frac{1}{2\rho N_0 + \gamma} \quad (26)$$

$$\overline{\delta N^2} = N_0 \times \left[\frac{(N_T + N_D - N_0)(N_0 - N_D)}{(N_T + N_D - N_0)(2N_0 - N_D) - N_0(N_0 - N_D)}\right] \quad (27)$$

Slightly Extrinsic In this case minority carriers are of importance. Let us consider the case of N_D fully ionized donors, as illustrated in Figure 6. Then, at any time it is

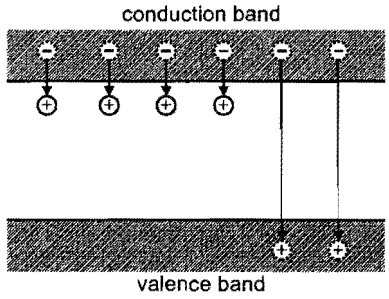

Figure 6. Energy band diagram and electron transitions involved in the fluctuations of conduction electrons in an n-type slightly extrinsic semiconductor with N_D the number of donors fully ionized, N the number of electrons in the conduction band, and P the number of minority holes in the valence band. Arrows indicate the direction of transition of an electron.

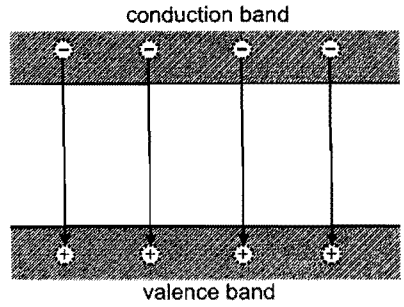

Figure 7. Energy band diagram and electron transitions involved in the fluctuations of conduction electrons in an intrinsic semiconductor with $N = P$ the number of electrons and holes.

$N = N_D + P$ carriers in the conduction band and P carriers in the valence band. Accordingly, we can write

$$g(N_0) = \gamma \tag{28}$$

$$r(N_0) = \rho N_0 P_0 = \rho N_0 (N_0 - N_D) \tag{29}$$

$$\tau_N = \frac{1}{\rho(N_0 + P_0)} \tag{30}$$

$$\overline{\delta N^2} = \overline{\delta P^2} = N_0 \times \left[\frac{P_0}{(N_0 + P_0)}\right] \tag{31}$$

and analogously for the acceptor case.

Intrinsic Semiconductors In this case, as illustrated in Figure 7, at any time it is $N = P$ and, for nondegenerate conditions, we can write

$$g(N_0) = \gamma \tag{32}$$

$$r(N_0) = \rho N_0 P_0 = \rho N_0^2 = \rho P_0^2 \tag{33}$$

$$\tau_N = \frac{1}{2\rho N_0} \tag{34}$$

$$\overline{\delta N^2} = \overline{\delta P^2} = \frac{N_0 P_0}{N_0 + P_0} = N_0 \times \left[\frac{1}{2}\right] \tag{35}$$

There may be fully ionized donors or fully filled acceptors which do not participate in transitions but contribute to charge balance, so that $(N - P) = (N_D - N_A)$.

Ambipolar Regime For the case of the ambipolar regime, typical of nearly intrinsic conditions when minority carriers become of importance, the lifetime of excess electron–hole pairs should be determined separately, and for the variance of electrons (in the case of an n-type sample) it is [21]

$$\overline{\delta N^2} = N_0 \times \left[\frac{N_0^2 P_0 (\mu_e + \mu_h)^2}{(N_0 + P_0)(\mu_e N_0 + \mu_h P_0)^2}\right] \tag{36}$$

with μ_e and μ_h the electron and hole mobility, respectively. An analogous expression holds for the case of a p-type sample.

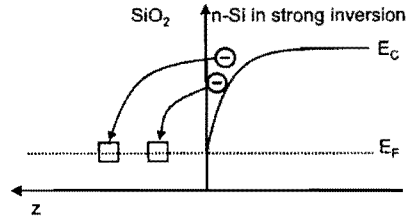

Figure 8. Energy band diagram and electron transitions involved in the fluctuations of N_0^-, the number of trapped electrons at the interface between a SiO_2 and an n-channel under strong inversion, with N_s the number of surface traps in the oxide.

N_s Surface Traps and N_0^- Trapped Electrons In this case, as illustrated in Figure 8, $g(N_0^-)$ is the trapping rate of electrons and $r(N_0^-)$ is their release rate from traps for which we can write

$$g(N_0^-) = \gamma(N_s - N_0^-) \tag{37}$$

$$r(N_0^-) = \rho N_0^- \tag{38}$$

$$\tau_{N^-} = \frac{1}{\rho + \gamma} \tag{39}$$

$$\overline{(\delta N_0^-)^2} = N_0^- \times \left[\left(1 - \frac{N_0^-}{N_s}\right)\right] \tag{40}$$

so that the fluctuations of the trapped follow a binomial law [4].

Real Space Transfer Consider a heterostructure consisting of two semiconductor materials, one (A) with a low energy gap and the other (B) with a large energy gap, as typified by the case of AlGaAs/GaAs/AlGaAs illustrated in Figure 9 where the energy diagram of a section of such a structure is reported. In the absence of an applied electric field most electrons reside in layer A where the potential energy is lower. Due to electron heating by an electric field and current flowing along the heterojunction (parallel transport) the electrons can transfer to the wide-gap layer B, where their mobility usually decreases. This transfer of electrons occurring in real space is known as "real space transfer" [22, 23]. It describes a spatial redistribution of electrons in the perpendicular direction of the heterostructure due to an accelerating electric

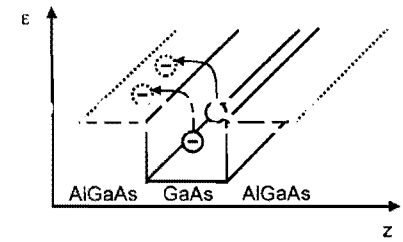

Figure 9. Energy band diagram and electron transfer in the real space from a GaAs layer to an adjacent AlGaAs layer during their parallel transport and heating in an external applied voltage.

field applied parallel to the direction of the structure. As a consequence of this mechanism, heterostructures can exhibit negative differential resistance with N-type shape. Furthermore, noise in these heterostructures can occur due to fluctuations of the electron concentration in various layers with different mobilities. The Vilnius group [24] has investigated the case of AlGaAs/GaAs/AlGaAs structures by providing evidence of this source of noise in terms of an anomalous behavior of the longitudinal diffusion coefficient which, as shown later in Section 2.5.1, can be interpreted in terms of GR noise.

Three-Level System and Shokley–Read–Hall Model By increasing the number of energy levels the complexity of statistical calculations increases rapidly. Below we report the results for the three-level system when transitions take place between the conduction band, the valence band, and one set of impurity centers N_I which may act as donors, acceptors, electron or hole traps, or recombination centers. Let I be the number of electrons in the impurity centers N_I. The condition of charge neutrality at any time imposes $N + I - P = C_0$ where C_0 is an appropriate constant number. In this case we have six transition rates coupling the three levels and for the variance of electrons, holes, and their cross term it is [3]

$$\overline{\delta N^2} = A_0\left(\frac{1}{P_0} + \frac{1}{I_0} + \frac{1}{N_I - I_0}\right) \tag{41}$$

$$\overline{\delta P^2} = A_0\left(\frac{1}{N_0} + \frac{1}{I_0} + \frac{1}{N_I - I_0}\right) \tag{42}$$

$$\overline{\delta N \delta P} = A_0\left(\frac{1}{I_0} + \frac{1}{N_I - I_0}\right) \tag{43}$$

where

$$A_0 = \left[\frac{1}{N_0 P_0} + \left(\frac{1}{I_0} + \frac{1}{N_I - I_0}\right)\left(\frac{1}{N_0} + \frac{1}{P_0}\right)\right]^{-1} \tag{44}$$

The Schokley–Read–Hall [25,26] model is obtained under the condition $I_0 \ll P_0$ or $(N_I - I_0) \ll N_0$ which implies

$$\overline{\delta N^2} \simeq \overline{\delta P^2} \simeq \overline{\delta N \delta P} \tag{45}$$

For further details concerning the time scales involved the reader should refer to the review [3].

2.2.2. *Momentum Space Representation*

With reference to a momentum representation of the band structure the GR processes can be specialized as follows.

Intervalley for Equivalent Valleys This mechanism is typical of covalent semiconductors (C, Si, and Ge) [27–31], where the conduction band is of many-valley type with ellipsoidal equienergetic surfaces, and the valence band is degenerate with heavy and light hole bands with warped equienergetic surfaces. The source of GR noise is the transfer of carriers between equivalent valleys for the case of electrons, as illustrated in Figure 10a and between degenerate bands for the case of holes, as illustrated in Figure 10b.

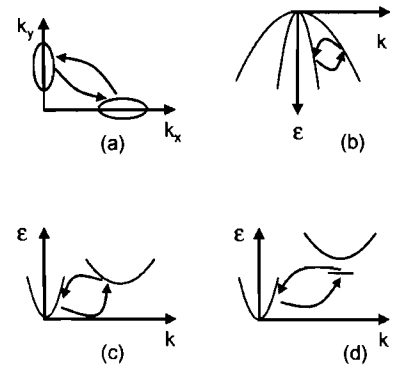

Figure 10. Schematic of transitions between different band states in momentum space typical of covalent and compound semiconductors. (a) Intervalley transfer between equivalent ellipsoidal valleys with different orientation in **k**-space. (b) Interband transfer between degenerate bands with different effective masses. (c) Intervalley transfer between nonequivalent valleys with different effective masses. (d) Transfer between continuum and resonant states.

Intervalley for Nonequivalent Valleys This mechanism is typical of compound semiconductors belonging to III–V (e.g., GaAs, InSb, InP, etc.) and II–VI (e.g., CdTe, ZnSe, etc.) groups [24]. In these materials the presence of satellite conducting band minima at energies above the bottom of the conduction band plays an important role for the transport properties at high applied fields. Figure 10c shows schematically this type of carrier transfer between nonequivalent minima which represents the source of GR noise.

Transition from Continuum to Resonant States This mechanism is also typical of compound semiconductors [24] and concerns the transfer of carriers from the conduction band minimum to localized states associated with satellite minima and back, as shown schematically in Figure 10d.

2.3. The Langevin Method

The Langevin method consists of adding to the equations of motion describing the relaxation of the relevant dynamic variables under study a random term representing the source of the fluctuations of each variable around its stationary value. The random term has an average value equal to zero and a proper value for its variance. In the following we briefly review the application of this method to the case of GR noise in order of increasing complexity.

2.3.1. *The Simple Two-Level Model*

For a simple two-level model with a conducting band and a donor level which provides majority carriers at thermal

equilibrium, the proper Langevin equation is obtained by adding to the continuity equation for conduction electrons number $N(t)$ a random noise source $L(t)$ as [3, 32–35]

$$\frac{dN(t)}{dt} = g(N) - r(N) + L(t) = -\frac{\delta N(t)}{\tau_N} + L(t) \quad (46)$$

where, in analogy with the standard theory of Section 2.1, it is $g - r \simeq -(r' - g')\delta N = \delta N/\tau_N$, $L(t)$ is the Langevin random source with zero average (i.e., $\overline{L(t)} = 0$), and the correlation function $C_L(t)$ is determined by the fluctuation dissipation theorem as

$$C_L(t) = \frac{\overline{\delta N^2}}{\tau_N}\delta(t) = \frac{1}{2}(g_0 + r_0)\delta(t) \quad (47)$$

where the last expression in the right-hand side (r.h.s) of Eq. (47) emphasizes the fact that the GR Langevin sources are shotlike. In the frequency domain, Eq. (47) implies a white spectral density of the Langevin source given by

$$S_L(\omega) = \frac{\overline{\delta N^2}}{\tau_N} = \frac{1}{\tau_N^2} S_N(0) \quad (48)$$

By assuming that transport and GR noise are independent, the GR current noise spectrum is thus constructed as

$$S_I^{\mathrm{GR}}(\omega) = I^2 \frac{S_N(\omega)}{N_0^2} \quad (49)$$

The case above can be analogously extended to the valence band and an acceptor level.

More rigorous approaches try to obtain the current (or voltage) noise spectra by including carrier transport since the beginning, thus coupling GR and velocity fluctuations in a consistent way. In the following sections we survey some of these attempts.

2.3.2. *The Coupled Langevin Equations*

In the presence of an applied electric field sufficiently high to induce hot carrier effects, carrier number fluctuations couple with velocity and energy fluctuations, making the simple decomposition procedure of different sources as in Eq. (2) not physically plausible. A coupled Langevin equation analysis of hot carriers was developed in [36, 37] for the case of cubic semiconductors and it was applied to the case of p-type Si. A current spectral density model was obtained [38] which, because of the presence of the field, becomes anisotropic with a longitudinal and two transverse components with respect to the current flow. For a spherical and parabolic band structure, the two transverse components coincide. The longitudinal component, $S_I^l(\omega)$, takes two different forms depending whether the velocity energy coupling is described by (I) two real distinct or (II) two complex conjugate rates. Accordingly, they take the form, respectively, for case I,

$$S_I^l(\omega) = \frac{B_1}{1 + (\omega\tau_u)^2} + \frac{B_2}{1 + (\omega\tau_{vl})^2} + \frac{B_3}{1 + (\omega\tau_\epsilon)^2} \quad (50)$$

or, for case II,

$$\begin{aligned} S_I^l(\omega) = {} & \frac{B_1}{1 + (\omega\tau_u)^2} \\ & + B_4\left[\frac{1}{1 + (\omega - \omega_0)^2\tau_0^2} + \frac{1}{1 + (\omega + \omega_0)^2\tau_0^2}\right] \\ & + B_5\left[\frac{(\omega + \omega_0)\tau_0}{1 + (\omega + \omega_0)^2\tau_0^2} - \frac{(\omega - \omega_0)\tau_0}{1 + (\omega - \omega_0)^2\tau_0^2}\right] \end{aligned} \quad (51)$$

The spectral density in the direction transverse to the current, $S_I^t(\omega)$, is a simple Lorentzian:

$$S_I^t(\omega) = \frac{B_6}{1 + (\omega\tau_{vt})^2} \quad (52)$$

The coefficients B_i, with dimensions A^2/Hz, give the strength of the respective noise sources. Since some of the B_i can have positive or negative values (as it is for B_3 and B_5) the respective noise sources can be enhanced or suppressed. The correspondent parameters τ_i^{-1} represent relevant rates associated with the decay of the fluctuation of the relevant ith variables (fraction of ionized carriers u, longitudinal velocity v_l, transverse velocity v_t, energy ϵ). We note that τ_0^{-1} and ω_0 are charateristic frequencies replacing τ_{vl}^{-1} and τ_ϵ^{-1} when there is a deterministic contribution in the transport regime (i.e., when $\tau_{vl} \simeq \tau_\epsilon$). Figure 11 illustrates the longitudinal spectral density and the associated correlation functions (see insets in Fig. 11) for the two cases given above. Figure 11a shows an example of a longitudinal spectral density belonging to case I. In this case the spectrum consists of the sum of two Lorentzians. Since the velocity relaxation time determines the highest cutoff frequency, B_2 is always positive, while B_3 can be in general positive or negative. A negative value is of particular interest because it leads to a spectral density whose maximum is not at low frequency but at some intermediate frequency between the energy and the velocity relaxation rate. Figure 11b shows an example of a longitudinal spectral density belonging to case II. In this case the two contributions can be classified as an "absorptive" contribution with coefficient B_4 and a "dispersive" contribution with coefficient B_5. The absorptive contribution must always be positive; this requires a positive B_4. The dispersive contribution changes its sign at the resonant frequency which, in the case of weak damping, is approximately given by ω_0. Even if the two spectra in Figure 11a and b are quite different, they exhibit the same main features in starting with a low-frequency plateau, then having a maximum, and finally decaying like a Lorentzian.

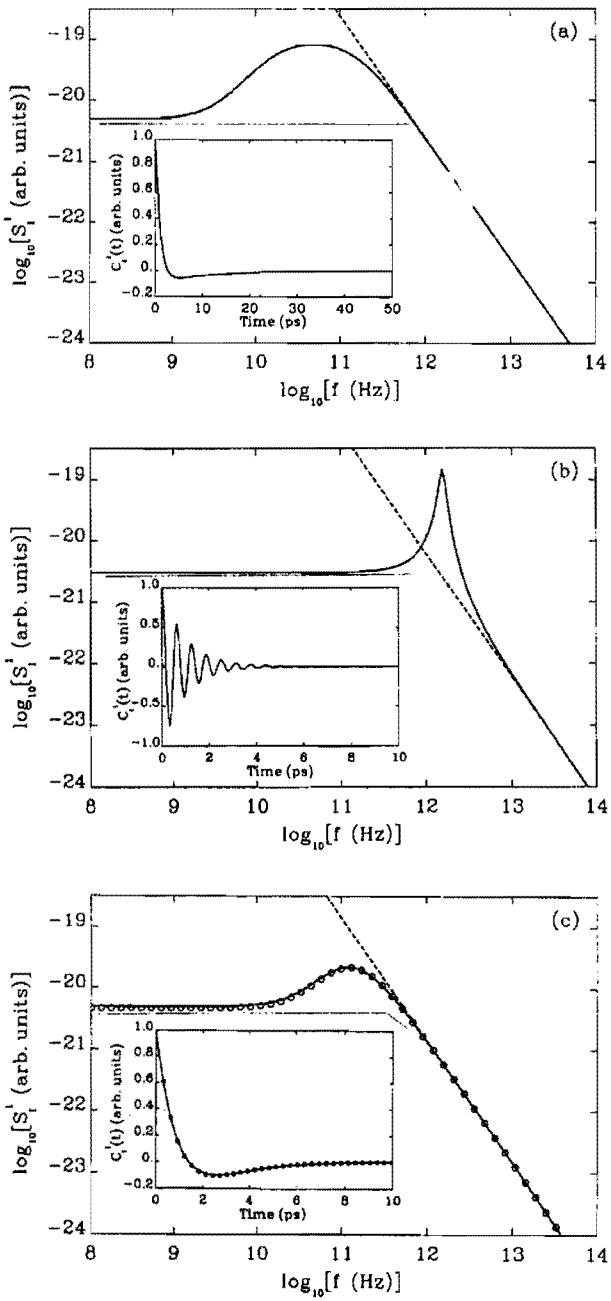

Figure 11. Model of the longitudinal current spectral density describing the coupling between velocity and energy fluctuations as a function of frequency. The insets display the corresponding correlation functions. (a) Spectrum and correlation function described by two real rates $1/\tau_{vl} = 10^{12}\ s^{-1}$, $1/\tau_\epsilon = 10^{11} s^{-1}$, $B_1/B_2 = -0.95$. (b) Spectrum and correlation function described by complex conjugate rates $\omega_0 = 10^{12} s^{-1}$, $1/\tau_0 = 10^{11} s^{-1}$, $B_3/B_4 = 0.01$ which correspond to the case of weak damping. (c) Spectrum and correlation function described by either of two real rates close together, $1/\tau_{vl} = 0.67 \times 10^{12}\ s^{-1}$, $1/\tau_\epsilon = 6.7 \times 10^{11} s^{-1}$ $B_1/B_2 = -0.95$, or by complex conjugate rates $\omega_0 = 8.3 \times 10^{10}\ s^{-1}$, $1/\tau_0 = 8.3 \times 10^{11}\ s^{-1}$, $B_3/B_4 = -0.89$. The dashed lines are the high-frequency asymptotes which separate the position of the maximum in the weak damping limit from the other cases.

Therefore, the question arises: Is there always a unique possibility to determine whether the spectral density has the form of Eq. (50) or (51)? In general the answer is no, as can be seen in Figure 11c. Here the solid line is calculated for case I while the circles are calculated for case II: there is a perfect agreement between the cases. There is an ambiguity if in case I the velocity and energy times are close to each other, this can be mapped to a spectral density of case II in the limit of strong damping ($\omega_0\tau_0 \ll 1$). On the other hand, two time scales τ_{vl} and τ_ϵ, very different in case I, lead to a broad maximum which cannot be reproduced by case II, while a sufficient weak damping in case II ($\omega_0\tau_0 > \sqrt{2}$) leads to a maximum above the high-frequency asymptote (shown as dashed lines in Fig. 11). In case I the maximum is always below the asymptote.

2.3.3. The Transfer Impedance Field Method

Introduced by Shockley et al. [39] as the impedance field method, this approach developed into the transfer impedance field method [40, 41] and successively was implemented by several authors [9, 42–47]. The general strategy of the method consists of factorizing the noise problem into two separate tasks aiming at determining (i) the noise source, responsible for the appearance of local fluctuations, and (ii) the transfer property of a local perturbation up to the structure terminals.

For a simple one-dimensional structure with constant cross section A and length L it is

$$S_V(\omega) = A\int_0^L dx \int_0^L dx' \int_0^L dx'' \int_0^L dx''' \, z(x, x'', \omega) \times K(x'', x''', \omega) z^*(x', x''', \omega) \tag{53}$$

where $z(x, x', \omega)$ is the transfer impedance matrix, that is, the Fourier transform of the Green function of the linearized electrical response around the bias point with the asterisk denoting complex conjugate, and $K(x', x'', \omega)$ is the two-point current spectral strength of fluctuations [45]. We recall that the small signal impedance $Z(\omega)$ is obtained as

$$Z(\omega) = \int_0^L dx \int_0^L dx' \, z(x, x', \omega) \tag{54}$$

By taking local uncorrelated current noise sources, for the GR contribution it is

$$K^{GR}(x, x', \omega) = \frac{j(x)^2}{n(x)} \frac{4\alpha(x)\tau_N(x)}{1 + (\omega\tau)^2} \delta(x - x') \tag{55}$$

with $\alpha(x) = \overline{\delta N(x)^2}/\overline{N(x)}$ a dimensionless parameter which describes the deviation of the local carrier number fluctuations from the full Poissonian behavior $\alpha(x) = 1$. The above expressions for K^{GR} represent a local generalization of the global expression entering Eq. (2).

2.4. The Master Equation Approach

The most general method to study fluctuations is to make use of the master equation, that is, an equation for the conditional probability [48] which, by determining the correlation function of the fluctuating quantity, implicitly contains the noise sources of the given problem.

2.4.1. A Simple Transport Model

Within the master equation approach, a simple transport model including the conduction band and an impurity level was developed in Ref. [49]. By considering noninteracting carriers under nondegenerate conditions three time scales are introduced at a phenomenological level as (i) the generation time τ_g, (ii) the recombination time τ_r, and (iii) the free carrier scattering time τ_s. From a macroscopic point of view, the above three times are combined to give (i) the momentum relaxation time, $\tau_m = \tau_s\tau_r/(\tau_s + \tau_r)$, (ii) the lifetime, $\tau_N = \tau_g\tau_r/(\tau_g + \tau_r)$, and (iii) the fraction of ionized carriers, $u = \tau_r/(\tau_g + \tau_r)$, which are the quantities used to interpret experiments. Then, the correlation function of current fluctuations takes the form

$$C_I(t) = \left(\frac{e}{L}\right)^2 N_0 \overline{\delta v(0)\delta v(t)} \tag{56}$$

with the correlation function of the velocity fluctuation of a single carrier given by

$$\begin{aligned}\overline{\delta v(0)\delta v(t)} = C_v(t) &= u\overline{\delta v_{fc}^2}\exp(-t/\tau_m) \\ &+ \overline{v_{fc}}^2 \frac{\tau_g}{(\tau_g - \tau_s)(\tau_g + \tau_r)^2} \\ &\times [\tau_g(\tau_r + \tau_s)\exp(-t/\tau_N) \\ &- \tau_s(\tau_g + \tau_s)\exp(-t/\tau_m)]\end{aligned} \tag{57}$$

where $\overline{v_{fc}} = e\tau_m E/m^*$ is the free carrier drift velocity, and $\overline{\delta v_{fc}^2} = K_B T_e/m^*$ is its variance expressed in terms of an electron temperature T_e associated with the carrier mean energy as $\bar{\epsilon} = (3/2)K_B T_e$. In the r.h.s. of the above equation, the first term gives the noise associated with velocity fluctuations, and the second term gives the noise associated with the GR contribution. Interestingly, the GR contribution consists of two parts which consistently couples scattering in the conduction band with the GR processes. The two limiting cases of interest are when $\tau_s \ll \tau_g, \tau_r$, which we shall call the additive mode, and the opposite case, $\tau_s \gg \tau_g, \tau_r$, which we shall call the mixing mode.

In the former case, $C_v(t)$ takes the form

$$C_v^{\text{add}}(t) = u\overline{\delta v_{fc}^2}\exp(-t/\tau_m) + u(1-u)\overline{v_{fc}}^2\exp(-t/\tau_N) \tag{58}$$

Thus, the values of τ_m and τ_N being far apart, the correlation functions associated with velocity and GR processes add independently.

In the latter case, $C_v(t)$ takes the form

$$C_v^{\text{mix}}(t) = \left[u\overline{\delta v_{fc}^2} + \overline{v_{fc}}^2 \frac{\tau_g\tau_s}{(\tau_r + \tau_s)^2}\right]\exp(-t/\tau_r) \tag{59}$$

Thus, both sources of fluctuation mix and a single relaxation time (i.e., the recombination time) describes the current fluctuations, and the GR contributes only to the amplitude of the correlation function. In experiments the former case is the most usual while, to our knowledge, no experiments are yet available for the latter case.

2.5. The Monte Carlo Method

By providing a kinetic solution of the carrier motion at a corpuscolar level, the Monte Carlo (MC) method offers the advantage of giving both the average values and the intrinsic fluctuations around the average associated with the stochastic nature of the individual microscopic processes, that is, the random scattering events [5, 20, 28, 38, 49–62]. By providing the instantaneous total current as measured in the external circuit $I(t)$ under steady state, the correlation function of current fluctuations is determined by recording $I(t)$ over a sufficiently long time period and, in turn, the associated spectral density is calculated by Fourier transform. In the following subsections the electronic noise is investigated when scattering both in the conducting band and in the GR processes between the conducting band and an impurity center are present [63, 64].

2.5.1. Decomposition of the Current Spectral Density

For the two-level model here considered, it is convenient to define the instantaneous value of the reduced velocity component in the field direction, $v_d^r(t) = u(t)v_d(t)$, with $v_d(t)$ the instantaneous carrier drift velocity. The presence of an applied electric field is in general responsible for a non-Ohmic velocity field characteristic also called hot-electron effects [30] which leads to an anisotropic behavior of the current or voltage fluctuation spectral density. As a consequence, a longitudinal, $S_I^l(\omega)$, and transverse, $S_I^t(\omega)$, components of the spectral density with respect to the direction of the applied field are introduced. The longitudinal component of the current spectral density is exactly decomposed into the sum of three terms which are related, respectively, to fluctuations in free carrier drift velocity (S_{Ivd}), number (S_{IN}), and correlation between number and velocity (S_{Icr}) as

$$\begin{aligned}S_I^l(\omega) &= 2\left(\frac{eN_0}{L}\right)^2 \int_{-\infty}^{+\infty} \exp(i\omega t)\overline{\delta v_d^r(0)\delta v_d^r(t)}\,dt \\ &= S_{Ivd}(\omega) + S_{IN}(\omega) + S_{Icr}(\omega)\end{aligned} \tag{60}$$

with

$$S_{Ivd}(\omega) = 2\left(\frac{eN_0}{L}\right)^2 \int_{-\infty}^{+\infty} \exp(i\omega t)\overline{\delta v_d(0)\delta v_d(t)}\,dt \tag{61}$$

$$S_{IN}(\omega) = 2\left(\frac{eN_0\overline{v_d}}{L\overline{u}}\right)^2 \int_{-\infty}^{+\infty} \exp(i\omega t)\overline{\delta u(0)\delta u(t)}\, dt \quad (62)$$

$$S_{Icr}(\omega) = 2\left(\frac{eN_0}{L}\right)^2 \frac{\overline{v_d}}{\overline{u}} \int_{-\infty}^{+\infty} \exp(i\omega t) \times \left[\overline{\delta u(0)\delta v_d(t)} + \overline{\delta v_d(0)\delta u(t)}\right] dt \quad (63)$$

Because of the cubic symmetry here considered, no transverse average current is present and the transverse component of the spectral density is given by

$$S_t'(\omega) = 2\left(\frac{e\overline{N}}{L}\right)^2 \int_{-\infty}^{+\infty} \exp(i\omega t)\overline{v_t(0)v_t(t)}\, dt \quad (64)$$

where $v_t(t)$ is the ensemble average of the carrier velocity in the transverse direction with respect to the applied field.

From their definition, it appears that S_{IN} and S_{Icr} are proportional to $\overline{v_d}^2$, and at least to $\overline{v_d}$, respectively. Therefore, they describe excess noise and, as expected, vanish at thermodynamic equilibrium and/or when the noise is evaluated perpendicular to the field direction, where $\overline{v_d}$ is equal to zero. Of course, S_{IN} and S_{Icr} are both zero when the traps are fully ionized, since it implies that at any time $\delta u(t) = 0$.

2.5.2. *The Case of Noninteracting Particles*

The calculation of the longitudinal current spectral density, and of the three terms into which it can be decomposed, is considerably simplified for the case of noninteracting particles. We note that carrier–carrier interaction does not only mean a direct scattering between two carriers, but also a correlation introduced by the occupancy factor of the impurity levels. Thus, for a single-particle simulation only a binomial statistic can be treated and, taking advantage of the reduced velocity fluctuations $\delta v^r(t) = u(t)v(t) - \overline{uv}$, it is obtained as

$$\overline{\delta v_d^r(0)\delta v_d^r(t)} = \frac{1}{N_I\overline{u}^2}\overline{\delta v^r(0)\delta v^r(t)} + \frac{\overline{v_d^r}^2}{N_I\overline{u}^4}\overline{\delta u(0)\delta u(t)} - \frac{\overline{v_d^r}}{N_I\overline{u}^3}\left[\overline{\delta u(0)\delta v^r(t)} + \overline{\delta v^r(0)\delta u(t)}\right] \quad (65)$$

with N_I the total number of impurity centers,

$$\overline{\delta u(0)^2} = \overline{u}(1-\overline{u}) \quad (66)$$

$$\overline{\delta u(0)\delta v_d(0)} = \overline{\delta v_d(0)\delta u(0)} = 0 \quad (67)$$

and, within an electron temperature model, $\overline{\delta v^r(0)^2} = K_B T_e/m^*$.

Table 1. Parameters for p-type Si used in Monte Carlo calculations. The hole effective mass takes into account the nonparabolicity and therefore it varies as a function of carrier mean energy between the given values.

Quantity	Value	Units
Effective mass m^*	0.53–1.26	m_0
Optical phonon equivalent temperature θ_0	750	K
Relative static dielectric constant ϵ_0	11.7	–
Density ρ_0	2.32	g/cm^3
Sound velocity v_s	6.53×10^5	cm/s
Acoustic deformation potential E_1^0	5	eV
Optical deformation potential $D_t K$	6×10^8	eV/cm
Equilibrium volume recombination rate B_{rec}	4.2×10^{-6}	cm^3/s^{-1}
Equilibrium generation rate γ	1.0×10^9	s^{-1}
Energy of the acceptor level ϵ_a	45	meV

2.5.3. *Two Level Model in p-Si*

As application of the MC method we report the results obtained for the case of lightly doped p-type Si at 77 K. By assuming an uncompensated sample, even at equilibrium freeze-out of impurities is present. Therefore, the noise spectra as a function of the applied electric field are analyzed within a two-level model accounting for the valence band and the acceptor levels. Calculations refer to acceptor concentrations $n_A = 4 \times 10^{14}$ and 3×10^{15} cm^{-3} and are compared with experiments [60, 65]. The parameters used in calculations are reported in Table 1.

Figure 12 reports the energy dependence of the scattering rates due to different mechanisms which are used

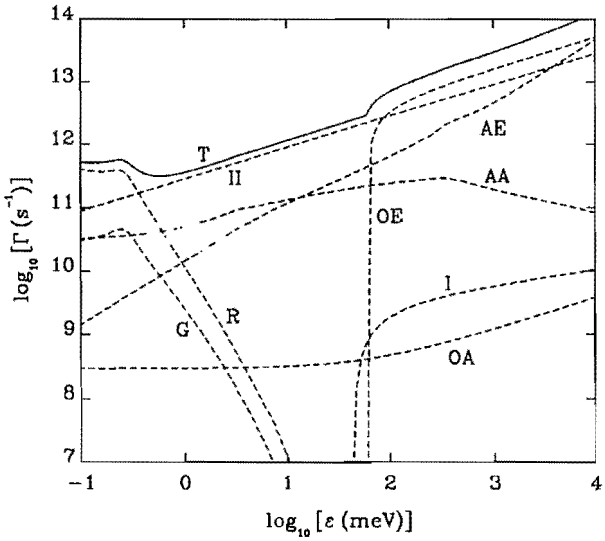

Figure 12. Scattering rates Γ as a function of carrier energy for p-type Si at 77 K with $n_A = 3 \times 10^{15}$ cm^{-1}. Symbols have the following meaning: AA (acoustic absorption), AE (acoustic emission), OA (optical absorption), OE (optical emission), II (ionized impurity), G (generation), I (impact ionization), R (recombination), T (total). Notice that the generation rate does not contribute to the total rate and that the energy scale refers to the final energy of the hole in the valence band.

in the calculations. We note that the generation (G) and recombination (R) rates dominate at the lowest energies while they decrease sharply at energies above about 0.2 meV.

The average fraction of ionized carriers is consistently determined from the ratio between the total time spent by a carrier in the valence band and the total time of the simulation. Then, both the generation rate and the average recombination rate are independently determined, respectively, from the ratio between the total time spent by a carrier inside the traps and the total number of generations and from the ratio between the total time spent inside the valence band and the total number of recombination processes.

Measured current spectral densities and the results of MC simulations are reported at various electric fields in Figure 13. We note that to account for the effect of using linear-recombination kinetics, the GR contribution is scaled by multiplying the value obtained from the simulation by a factor $(2 - \overline{u})^{-2}$. The initial increase with field of the spectral density is mainly due to the GR contribution which depends quadratically on the drift velocity. The final decrease is associated with the fact that

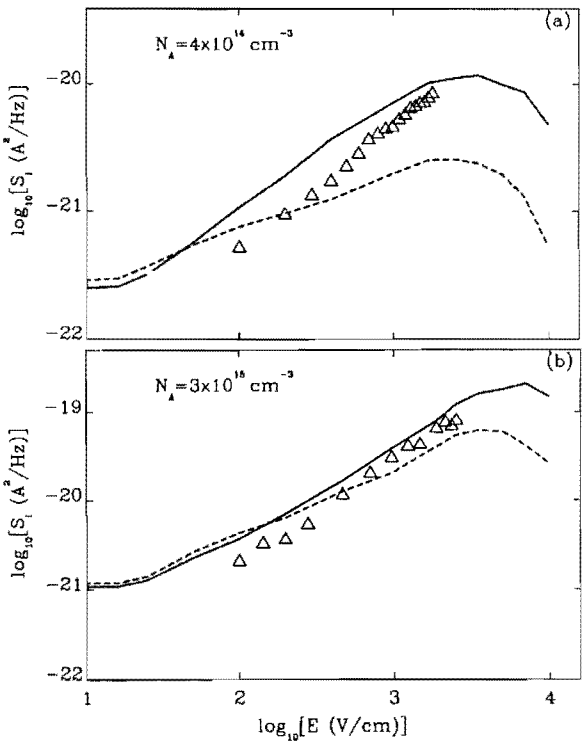

Figure 13. Low-frequency current spectral density as a function of the electric field for p-type Si at 77 K with (a) $n_A = 4 \times 10^{14}$ cm^{-3} and (b) $n_A = 3 \times 10^{15}$ cm^{-3}. Symbols refer to experiments obtained at the lowest frequency of 220 MHz, and curves refer to MC calculations. The dashed lines refer to a value of $\gamma = 2.9 \times 10^9$ s^{-1} and the solid line refers to a value of $\gamma = 10^9$ s^{-1}.

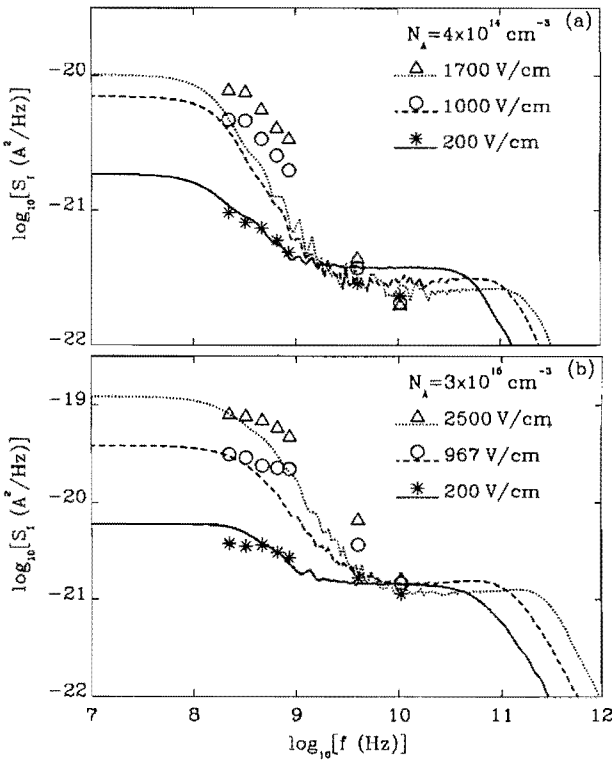

Figure 14. Current spectral density as a function of frequency for p-type Si at 77 K with (a) $n_A = 4 \times 10^{14}$ cm^{-3} and (b) $n_A = 3 \times 10^{15}$ cm^{-3} at different electric fields. Symbols refer to experiments and curves to MC calculations with $\gamma = 10^9$ s^{-1}.

practically all impurities are ionized at the highest fields and therefore the GR contribution reduces significantly.

The full spectrum of the current spectral density is reported in Figure 14 for three values of the electric field at each acceptor concentration. The spectra exhibit a strong frequency dependence, with apparently the end of the low-frequency GR noise plateau below 200 MHz, and the beginning of the high-frequency velocity noise plateau above 40 GHz. The cutoff frequency for GR is of the order of 0.70 GHz for the sample with $N_A = 4 \times 10^{14}$ cm^{-3}, and 1.3 GHz for the sample with $N_A = 3 \times 10^{15}$ cm^{-3}, corresponding to lifetimes of 0.23 and 0.12 ns, respectively. Such short lifetimes suggest that shallow traps are responsible for GR noise. The increase of the highest cutoff frequency with increasing field reflects the decrease of the mobility which is associated with the onset of hot carrier conditions. For the cases considered above, the theory well reproduces the main features of the experiments and agrees with them within a factor of two at worst. We note that the model satisfactorily interprets first-order quantities like the average free carrier concentration and the conductivity as functions of the applied field [56].

2.5.4. *Multilevel Model in p-Si*

Here we report a theoretical study of GR processes from shallow impurities which includes self-consistently the contribution of the impurity excited levels [53, 58, 63, 64]. The dynamics of GR processes was investigated at a kinetic level and the theory was based on MC simulations which account for both the kinetic energy of the carrier and the potential energy of the impurity. Calculations were performed for the case of p-type Si at temperatures below 100 K where freeze-out of impurity centers is significant.

Figure 15 reports the spectral density of number fluctuations [in terms of ionized fraction $S_u(f) = u^2 N_I/(2I^2) \times S_{IN}(f)$] at different doping concentrations and temperatures. The presence of excited levels is found to weaken the turning from a $1/f^2$ Lorentzian spectra into a region of nearly $1/f$ type of spectrum in the region of high frequencies centered around 1 GHz. This behavior extends over two decades before achieving the plateau region at the lowest frequencies. A significant result of the theory is the clear evidence of a nonexponential distribution of the microscopic times spent by carriers in both the impurity center and the conducting band.

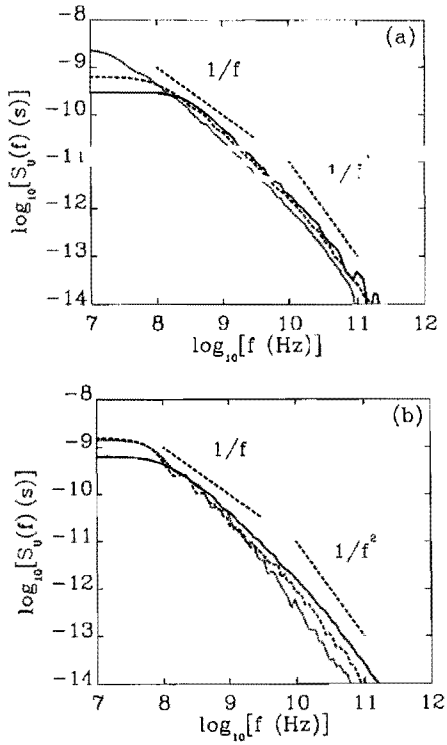

Figure 15. Spectral density of number fluctuations (in terms of the fraction of ionized carriers) obtained for the case of p-type Si at thermodynamic equilibrium. Together with the spectral density, the behaviors $1/f$ and $1/f^2$ are shown as guides to the eye. (a) refers to $T = 77$ K and the continuous, dashed, and dotted lines refer, respectively, to $n_A = 4 \times 10^{14}$, 3×10^{15}, and 1×10^{16} cm^{-3}. (b) refers to $n_A = 3 \times 10^{15}$ cm^{-3} and the continuous, dashed, and dotted lines refer, respectively, to $T = 77$, 50, and 10 K.

2.6. Other Theoretical Approaches

Below we briefly summarize existing theoretical approaches which have been developed and applied to investigate GR noise in semiconductor devices and which complement and/or implement the approaches presented in the previous sections. The partial differential equation method based on the introduction of appropriate Langevin sources within a transfer field approach was mostly developed by the Torino group and is now surveyed in a comprehensive textbook [9]. The scattered packet method, based on the solution of the kinetic equation, was developed by the Montpellier group [65, 66]. A percolative technique based on a random resistor network in which each resistor can be broken (recombination) and recovered (generation) according to given probabilities was developed by the Lecce group [67, 68]. The relaxation matrix approach for a three-level system in the presence of a high electric field was developed in Ref. [69]. A trapping noise model allowing for the determination of the noise spectrum as function of the trap position was developed by the Milano group [70]. The influence of the doping profile on deep level trap characteristics on GR noise was investigated in Ref. [71]. A Monte Carlo analysis of the influence of DC conditions on the up-conversion of GR noise in semiconductors was developed by the Salamanca group [72]. Generation–recombination noise has been implemented in an advanced device simulator, the Dessis-ISE package, which is commercially available, by the Zurich group [73]. We finally note that in some cases there is the possibility of interpreting GR within a generalized diffusion approach. The following subsection briefly review significant results on this attempt.

2.6.1. *The Generalized Diffusion Approach*

In the absence of two-particle interaction, relevant expressions describing GR noise in terms of a generalized diffusion coefficient for a two-level system concern the cases of (i) GR from traps and (ii) GR from intervalley scattering.

In the former case, the low-frequency spectral density of current fluctuations can be exactly decomposed as [53]

$$S_I(0) = \frac{4e^2 N_0}{L^2}[uD_{\rm vf} + D_{\rm gr} + D_{\rm cross}] \tag{68}$$

with D_i the diffusion coefficient related to velocity fluctuations ($i = $ vf), GR ($i = $ gr), and their cross-correlation ($i = $ cross), respectively. Interestingly, within a relaxation time approximation, the diagonal terms are written as

$$D_{\rm vf} = \overline{v^2}\tau_m \tag{69}$$

$$D_{\rm gr} = \frac{\overline{\delta N^2}}{N_0} v_d^2 \tau_N \tag{70}$$

In the latter case of intervalley processes between two valleys it is [27,28]:

$$S_I = \frac{4e^2 N_0}{L^2}[u_1 D_{vf1} + u_2 D_{vf2} + D_{int}] \tag{71}$$

with u_1 and $u_2 = (1 - u_1)$ the fraction of carriers in each valley and where, within a relaxation time approximation, it is

$$D_{int} = u_1 u_2 (\overline{v_1} - \overline{v_2})^2 \tau_{int} \tag{72}$$

with $\overline{v_{1,2}}$ the average velocity of carriers in valley 1 and 2, respectively, and τ_{int} the average time associated with intervalley transitions. We note the vectorial character of the average velocity which is responsible for an "intervalley" noise source in the direction perpendicular to the applied field for the case of ellipsoidal equienergetic surfaces when the current associated with a single valley contains a component perpendicular to the applied field. Figure 16 illustrates the microscopic mechanism responsible of the longitudinal and the transverse intervalley diffusion for a simplified two-valley model. Finally, we observe that Eq. (72) can be used for the real space GR noise with u_1 and u_2 indicating the fraction of carriers in the low and high energy gap regions of the heterostructure, respectively, as discussed in Section 2.2.2.

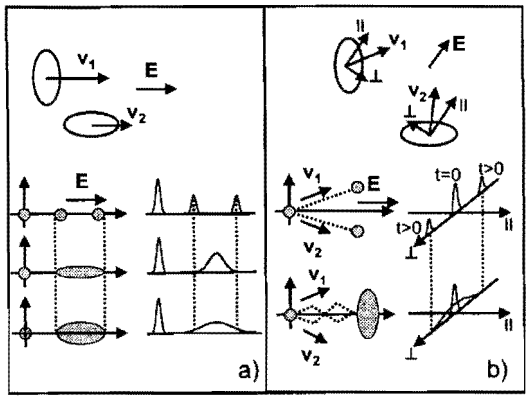

Figure 16. Phenomenology of the longitudinal (a) and transverse (b) intervalley diffusion in a simplified two-valley model. The upper part of the figures shows the orientation of the drift velocities pertaining to each valley v_1 and v_2 with respect to the driving field E. The lower parts of the figures show the time evolution of the spatial distribution for a bunch of carriers starting in position $x = 0$ at $t = 0$. The three evolutions reported in (a), from top to bottom, refer to the absence of any diffusion, the presence of intervalley diffusion only, and the presence of both intervalley and intravalley diffusion, respectively. The two evolutions reported in (b), from top to bottom, refer to the absence of any diffusion and to the presence of both intervalley and intravalley diffusion, respectively. Notice that in case (a) the intervalley diffusion contributes to the longitudinal current spectral density, while in case (b) the intervalley diffusion contributes to the transverse current spectral density.

3. EXPERIMENTS

The characterization of material and devices from GR noise measurements is a standard and well assessed technique which enables a noise spectroscopy of traps to be carried out [7]. In the presence of a single trapping level, the measurement of the generation time can give information on the charateristic energy of the trap and that of the recombination time on the scattering cross section, as can be deduced from the expressions developed in Section 2.5.1. The presence of two or more trapping levels modulates the frequency dependence of the noise spectrum. As a typical example, Figure 17 reports a voltage spectral density of an heavily doped p-type GaAs transmission line model [74]. Here two GR levels are individuated in the decomposition procedure which evidence $1/f$ and Nyquist contributions also. The spectral densities corresponding to excess noise show a quadratic dependence with bias current. For the case of p-type Si the analysis of GR noise has evidenced up to seven different trap centers [75]. Among materials evidencing GR noises from single and/or multiple traps we cite: hydrogenated amorphous Si [76], p-type GaN [77], CdHgTe epilayers [78], and n-type bulk 4H SiC [79]. Lorentzian modulated shot noise was found in the AlGaAs/GaAs quantum well [80].

Generation–recombination noise was investigated in many devices as can be seen from the "Proceedings of the International Conference on Noise in Physical Systems and $1/f$ Fluctuations" [81–86]. Here we cite the noise correlation measurements in bipolar transistors [87,88], in quantum well photodetectors biased to strong electric fields [89] and in quantum dot photodetectors [90,91], in p–n–p polysilicon emitter bipolar junction transistors [92], and in AlGaN/GaN heterojunction field effect transistors [93].

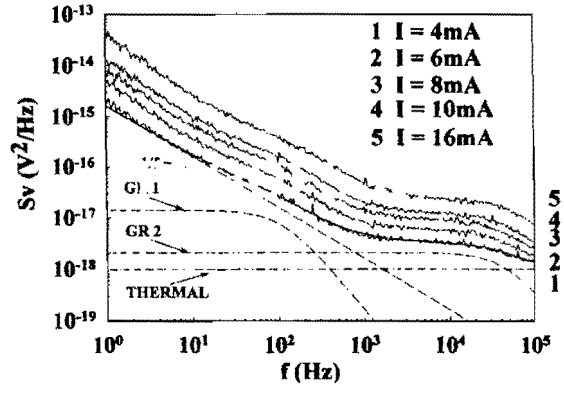

Figure 17. Voltage spectral density for various bias currents of a heavily doped p-type GaAs transmission line model with a length between contacts $L = 30\,\mu$m and a doping of $p = 4 \times 10^{19}$ cm^{-3}. Also reported in the figure is the decomposition of the spectral density number 1 into the different components $1/f$, two GR sources, and Nyquist. Reprinted with permission from [74]. © 1996, American Institute of Physics.

4. MISCELLANEA

Since its discovery, GR noise has emerged as a relevant noise source able to account for a variety of fluctuation properties when properly generalized. Below we report on four significant examples aiming at this purpose.

4.1. GR and RTS

The random telegraph signal (RTS) refers to a purely random signal which may be in one of the two states, called 1 or 0. Since its application to semiconductors [94], it has provided a useful interpretation of excess noise when this last is controlled by a single two-level fluctuator, as for the case of GR from a single trap. Generation and recombination from a single trap can be easily detected in submicron metal–oxide–semiconductor field effect transistors. Here, because of the small number of carriers involved in transport (of the order of a few thousands or less), giant fluctuations of the current can be easily monitored, as shown in Figure 18 where a typical RTS obtained by the Montpellier group [95] is reported. Following the general model for independent pulse [94], the low-frequency current spectral density associated with a RTS, $S_I^{\mathrm{RTS}}(\omega)$, takes the simple form

$$S_I^{\mathrm{RTS}}(0) = \frac{4\tau_g\tau_r}{(\tau_g+\tau_r)^2}\tau_N(\Delta I)^2 \tag{73}$$

with ΔI the amplitude of the RTS current pulse [18]. From the experimental RTS one can obtain separately the generation and the recombination times together with their statistics which can be compared with theoretical expectations.

4.2. From GR to $1/f$ Noise

Following the original suggestion of Bernamont [96], the superposition of GR sources with lifetime distributed on a logarithmic wide time scale with extrema τ_1 and τ_2 is known to give a $1/f$ spectrum in the intermediate range of frequencies $1/\tau_2 < \omega < 1/\tau_1$. To this purpose, by introducing a density distribution of lifetimes as $g(\tau_N)$ the spectral density of number fluctuations takes the form

$$S_N(\omega) = 4\overline{\delta N^2}\int_{\tau_1}^{\tau_2} g(\tau_N)\frac{\tau_N}{1+(\omega\tau_N)^2}d\tau_N \tag{74}$$

which, for $g(\tau_N) = [\tau_N \ln(\tau_2/\tau_1)]^{-1}$, gives a $1/f$ spectrum inside the regions determined by the limiting values of τ_N. We note that shape of $g(\tau)$ different from the simple hyperbolic form can be used to model the frequency dependence found in the experiments.

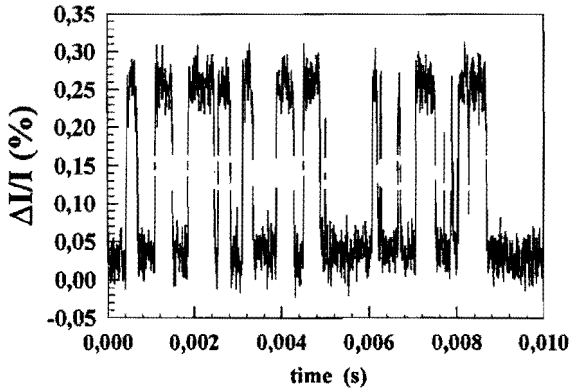

Figure 18. RTS current pulses observed in a poly-Si bipolar transistor with a 4.8 μm^2 emitter area at a base bias current of 0.5 μA. Reprinted with permission from [95]. © 2001, World Scientific.

4.3. From GR to Shot Noise

For the case of a strong extrinsic semiconductor in the presence of freeze-out the GR noise can exhibit a linear dependence with external current; that is, it becomes shot noise [3, 21, 97]. This happens when the transit time $\tau_T = L/v_d$ becomes the shortest time scale as compared with the lifetime of the GR process and the dielectric relaxation time, $\tau_d = \epsilon_r\epsilon_0/(en\mu)$ with n the carrier concentration and μ the carrier mobility. Indeed, the above condition implies that the total number of carriers inside the sample fluctuates in time because of the random entering and exiting process of carriers from contacts. The low-frequency spectral density of number fluctuations covering continuously the transition from GR (i.e., $\tau_d \gg \tau_N$) to shot noise (i.e., $\tau_d \ll \tau_N$) is found to be given by [3]

$$S_N(0) = 4\overline{\delta N^2}\tau_N\left\{1+\frac{\tau_N}{\tau_T}\left[\exp\left(-\frac{\tau_T}{\tau_N}\right)-1\right]\right\} \tag{75}$$

A similar situation may happen in the case of an ambipolar regime typical of near intrinsic semiconductors [21]. Then, for an n-type semiconductor an analogous expression like Eq. (75) holds with the ambipolar transit time $\tau_a = [L(\mu_e N_0 + \mu_h P_0)]/[|N_0 - P_0|\mu_e\mu_h E]$ replacing the unipolar transit time τ_T and with δN^2 given by $N_0P_0/(N_0+P_0)$.

4.4. GR as a General Approach to Noise

By replacing the energy space with the real space, the concept of generation–recombination can be fruitful extended to treat noise in arbitrary two-terminal devices limited by ideal contacts acting as a thermal reservoir at different electrochemical potentials [98–100]. Accordingly, by considering the emission of carriers from the contacts into the device and the collection of carriers from the device into the contacts as generation and recombination processes, respectively (see Fig. 19), the instantaneous current and its fluctuations can be described in terms of a master equation for the probability $P(N)$ of finding $N(t)$ electrons into the device at time t in complete analogy with the GR processes between different energy band states. The instantaneous current

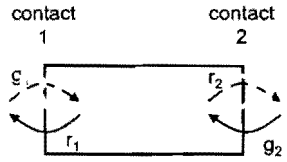

Figure 19. Schematic of current noise in a two-terminal device described by the stochastic character of emission (i.e., generation) and collecting (i.e., recombination) processes of carrier entering and leaving the device from opposite contacts.

at the emitter I_1 and collector I_2 interface with the device are given, respectively, by

$$I_1 = -e\sum_N [g_1(N) - r_1(N)]P(N) \tag{76}$$

$$I_2 = -e\sum_N [r_2(N) - g_2(N)]P(N) \tag{77}$$

where $g_1(N)$, $r_1(N)$ are the probability per unit time for electron transfer from the emitter into the device and from the device into the emitter, respectively. Analogously, $g_2(N)$, $r_2(N)$ are those from the collector to the device and from the device to the collector, respectively. Under stationary conditions the currents I_1 and I_2 are related by

$$\overline{I_1} = \overline{I_2} = \overline{I} \tag{78}$$

Their correlators can be constructed by introducing $P(N, t; M, 0)$ as the conditional probability of finding in the device N electrons at time t, given that M electrons were in the device at the previous time $t = 0$. As an example, in the high voltage case for which $g_2 = 0$ for the correlation function of the stationary current flowing in a two terminal device, $\overline{I(0)I(t)}$, it is found [100] that

$$\overline{I(0)I(t)} = \sum_{M,N} r_2(M)P(M)r_2(N)P(N, t; M-1, 0) \tag{79}$$

The solution of both the current–voltage and noise characteristics is thus concerned with a proper modeling of the generation–recombination rates for the problem under interest. The application of this theoretical approach has provided interesting results in the recent field of shot noise in mesoscopic devices [98–100].

5. FINAL CONCLUSIONS

We have presented a brief survey of generation and recombination noise in semiconductors with the objective of emphasizing some of the crucial aspects of this subject. A large amount of experimental data have accumulated since the announcement of this noise source made in the late 1950s, and the reader can refer for details to the "Proceedings of the International Conferences on Noise in Physical Systems and $1/f$ Fluctuations," which is held every two years [81–86]. Furthermore, cited books [4, 7–9] and reviews [3, 5, 6, 18] can complete the wide picture of the subject. Different mechanisms responsible for this noise are here illustrated with reference to the representation of semiconductor electron energy levels in real and momentum space. The main theoretical approaches are briefly recalled in order of increasing complexity. Accordingly, the master equation for number fluctuations, the Langevin method and the impedance field method in the presence of carrier transport, and the MC method at a kinetic level are identified as the basic theoretical approaches. The application of the MC method to the case of p-Si is reported as a significant example of a microscopic interpretation of GR in the presence of an external electric field. Excerpts of significant experiments concerning GR noise are mentioned for a variety of physical systems. The extension of the initial concept of generation–recombination noise to cover other noise phenomena, like $1/f$ noise, random telegraph noise, shot noise, and in general the noise in two terminal devices, is outlined.

ACKNOWLEDGMENTS

We gratefully acknowledge the support from the MADESS II project of the Italian National Research Council (CNR) and the Galileo Project 99055.

LIST OF SYMBOLS

A	Cross-sectional area of a two-terminal device
A_0	Constant entering the statistics of the three-level system
a	Numerical parameter for the Poole–Frenkel effect
$\alpha(x)$	Dimensionless parameter describing the deviation of the local carrier number fluctuations from Poissonian behavior
B_{eq}	Volume recombination rate at thermal equilibrium
B_i	Strength of the ith relevant noise source of the coupled Langevin equations
β	Poole–Frenkel constant
C	Strength of $1/f$ fluctuations
$C_I(t)$	Correlation function of current fluctuations
$C_L(t)$	Correlation function of the random Langevin force
$C_N(t)$	Correlation function of number fluctuations
C_0	Given number of carriers
$C_v^{add}(t)$	Correlation function of the single carrier velocity fluctuations in the

	generation–recombination additive mode
$C_v^{\text{mix}}(t)$	Correlation function of the single carrier velocity fluctuations in the generation–recombination mixing mode
D_i	Diffusion coefficient associated with the ith process
E	Electric field
E_c	Energy of the conducting band edge
e	Unit electron charge
ϵ	Carrier energy
$\bar{\epsilon}$	Average carrier energy
ϵ_D	Energy of the impurity level relative to the conduction band edge
ϵ_r	Relative static dielectric constant
ϵ_0	Vacuum permittivity
f	Frequency
G	Conductance
g_D	Spin degeneracy factor
$g(N)$	Generation probability per unit time
$g(\tau_N)$	Density distribution of lifetimes
g_0	Generation probability per unit time under stationary conditions
g_1	Probability per unit time for electron transfer from the emitter into a two-terminal device
g_2	Probability per unit time for electron transfer from the collector into a two-terminal device
γ	Generation rate strength
γ_{eq}	Generation rate strength at thermal equilibrium
γ^{PF}	Generation rate strength in the presence of the Poole–Frenkel effect
I_0	Average number of electrons occuping an N_I center
$I(t)$	Instantaneous current
$\overline{I}$	Average value of the current
$I_1(t)$	Instantaneous current at the emitter contact of a two-terminal device
$\overline{I_1}$	Average value of the current at the emitter contact of a two-terminal device
$I_2(t)$	Instantaneous current at the collector contact of a two-terminal device
$\overline{I_2}$	Average value of the current at the collector contact of a two-terminal device
$\overline{I(0)I(t)}$	Correlation function of the stationary current flowing into a two-terminal device
ΔI	Amplitude of a random telegraph signal
$j(x)$	Current density
$K(x', x'', \omega)$	Two-point current spectral strength of fluctuations
$K^{\text{GR}}(x', x'', \omega)$	Two-point current spectral strength of fluctuations associated with generation–recombination noise
K_B	Boltzmann constant
L	Length of a two-terminal device
$L(t)$	Langevin force for number fluctuations
m^*	Effective mass
μ	Carrier mobility
μ_e	Electron mobility
μ_h	Hole mobility
$N(t)$	Number of instantaneous free carriers
N_0	Average number of electrons in the conduction band
N_A	Number of acceptors
N_D	Number of donors
N_I	Number of impurity centers acting as trapping and/or recombination levels
$N_N = 4.83 \times 10^{21}\ \text{m}^{-3}\text{K}^{-3/2}$	Universal constant
N_T	Number of partially ionized donor traps
$\overline{\delta N^2}$	Variance of carrier number fluctuations
N_s	Average number of surface traps
N_t	Number of partially ionized donor traps
N_0^-	Number of trapped electrons
$\overline{(\delta N_0)^2}$	Variance of the number of electrons trapped in the surface traps
n	Free electron concentration
n_D	Donor concentration
$P(N)$	Probability distribution of finding N electrons inside the sample at time t
$P(N, t; M, 0)$	Conditional probability distribution to find in the device N electrons at time t, given that M electrons were in the device at time $t = 0$
P_0	Average number of holes in the valence band
R	Resistance
$r(N)$	Recombination probability per unit time
r_0	Recombination probability per unit time under stationary conditions
r_1	Probability per unit time for electron transfer from a two-terminal device into the emitter contact
r_2	Probability per unit time for electron transfer from a two-terminal device into the collector contact
ρ	Recombination rate strength
ρ_{eq}	Recombination rate strength at thermal equilibrium

$S_G(\omega)$	Spectral density of conductance fluctuations
$S_I(\omega)$	Spectral density of total current fluctuations
$S_L(\omega)$	Spectral density of the random Langevin force
$S_N(\omega)$	Spectral density of carrier number fluctuations
$S_R(\omega)$	Spectral density of resistance fluctuations
$S_V(\omega)$	Spectral density of voltage fluctuations
$S_{Ivd}(\omega)$	Spectral density of current fluctuations associated with fluctuations of the free carier drift velocity
$S_I^{GR}(\omega)$	Current spectral density associated with generation–recombination noise
$S_{IN}(\omega)$	Spectral density of current fluctuations associated with fluctuations of the number of free carriers
$S_I^{RTS}(\omega)$	Current spectral density associated with a random telegraph signal
$S_I^l(\omega)$	Longitudinal current spectral density
$S_I^t(\omega)$	Transverse current spectral density
$S_{Icr}(\omega)$	Spectral density of current fluctuations associated with correlated fluctuations of the free carrier drift velocity and their number
$\sigma(\epsilon)$	Microscopic capture cross section
T	Bath temperature
T_e	Electron temperature
τ_N	Lifetime of electrons in the conduction band
τ_T	Transit time
τ_{N^-}	Lifetime of electrons trapped in the surface states
τ_a	Ambipolar transit time
τ_d	Dielectric relaxation time
$1/\tau_g$	Generation rate
τ_i^{-1}	Relevant rates associated with the ith relevant dynamic variable
$1/\tau_r$	Recombination rate
τ_s	Free carrier scattering time
u	Fraction of ionized carriers
u_{eq}	Fraction of ionized carriers at thermal equilibrium
u_i	fraction of carrier associated with the ith valley
$\overline{\delta u^2}$	Variance of the fraction of ionized carrier number fluctuations
V	Voltage
v_0	Carrier thermal velocity
$v_d(t)$	Instantaneous value of the drift velocity component in the field direction
$\overline{v_d}$	Average value of the drift velocity component in the field direction
$v_d^r(t)$	Instantaneous value of the reduced velocity component in the field direction
$\overline{v_d^r}$	Average value of the reduced velocity component in the field direction
$\overline{(\delta v_d^r)^2}$	Variance of the reduced velocity fluctuation in the field direction
$\overline{\delta v_{fc}^2}$	Variance of the drift velocity fluctuation in the direction of the electric field
$v_{fc}(t)$	Instantaneous free carrier drift velocity
$\overline{\mathbf{v}_i}$	Average carrier velocity associated with the ith valley
$Y(\omega)$	Small signal admittance
$Z(\omega)$	Small signal impedance
$z(x, x', \omega)$	Transfer impedance matrix
$\omega = 2\pi f$	Circular frequency

REFERENCES

1. C. vanVliet, in "Noise in Physical Systems and $1/f$ Fluctuations", (C. Surya, Ed.), p. 3. Bentham Press, London, 1999.
2. A. van der Ziel, "Noise." Prentice-Hall, New York, 1954.
3. K. vanVliet and J. Fassett, in "Fluctuation Phenomena in Solids," (R. Burgess, Ed.), p. 267. Academic, New York, 1965.
4. A. van der Ziel, "Noise in Solid State Devices and Circuits." Wiley, New York, 1986.
5. L. Reggiani and V. Mitin, *Riv. Nuovo Cimento* 12, 1 (1989).
6. L. Reggiani and L. Varani, *Riv. Nuovo Cimento* 17, 1 (1994).
7. N. Lukyanchikova, in "Noise Research in Semiconductor Physics" (B. Jones, Ed.), Gordon and Breach, Amsterdam, 1996.
8. S. Kogan, "Electron Noise and Fluctuations in Solids. Cambridge Univ. Press, Cambridge, UK, 1996.
9. F. Bonani and G. Ghione, "Noise in Semiconductors Devices, Modeling and Simulation." Springer-Verlag, Berlin, 2001.
10. H. Nyquist, *Phys. Rev.* 32, 110 (1928).
11. V. Bareikis, V. Viktoravichyus, and A. Galdikas, *Sov. Phys. Semicond.* 16, 1202 (1982).
12. V. Bareikis et al., *IEEE Trans. Electron Devices* 41, 2051 (1994).
13. B. Jones, *IEEE Trans. Electron Devices* 41, 2188 (1994).
14. H. Pool, *Philos. Mag.* 32, 112 (1916).
15. J. Frenkel, *Phys. Rev.* 54, 647 (1938).
16. V. Kozub, *Sov. Phys. Solid State* 26, 1186 (1984).
17. C. Rogers and R. Burman, *Phys. Rev. Lett.* 53, 1272 (1984).
18. M. Kirton and Uren, *Adv. Phys* 38, 367 (1989).
19. R. Burgess, *Proc. Phys. Soc. London Sect. B* 69, 1020 (1956).
20. T. Kuhn, L. Reggiani, L. Varani, and V. Mitin, *Phys. Rev. B* 42, 5702 (1990).
21. J. E. Hill and K. M. vanVliet, *Physica* 24, 709 (1958).

22. A. van Die and J. Dijkhuis, *J. Appl. Phys.* 74, 1143 (1993).
23. Z. Gribnikov, K. Hess, and G. Kosinovsky, *J. Appl. Phys.* 77, 1337 (1995).
24. V. Aninkevicius et al., *Phys. Rev. B* 53, 6893 (1996).
25. W. Shockley and W. T. Read, *Phys. Rev.* 87, 835 (1952).
26. R. N. Hall, *Phys. Rev.* 87, 387 (1952).
27. P. Price, in "Fluctuation Phenomena in Solids" (R. Burgess, Ed.), p. 249. Academic, New York, 1965.
28. R. Brunetti et al., *J. Appl. Phys.* 52, 6713 (1981).
29. R. Brunetti, C. Jacoboni, and L. Reggiani, *J. Phys. Suppl.* 10 42, C7 (1981).
30. L. Reggiani, "Hot-Electron Transport in Semiconductors", Vol. 58 of Topics in Applied Physics. Springer, Berlin, 1985.
31. V. Mitin and C. vanVliet, *Phys. Rev. B* 41, 5332 (1990).
32. K. vanVliet, *Phys. Rev.* 110, 50 (1958).
33. K. vanVliet, in "Proceedings of the 7th Internat. Conf. on the Physics of Semiconductors," Dunod, Paris, 1964, p. 831.
34. C. vanVliet, private communication, Modena, 1991.
35. C. vanVliet, *IEEE Trans. Electron Devices* 41, 1902 (1994).
36. T. Kuhn, L. Reggiani, and L. Varani, *Phys. Rev. B* 45, 1903 (1992).
37. L. Reggiani, T. Kuhn, and L. Varani, *Semicond. Sci. Technol.* 7, 8364 (1992).
38. T. Kuhn, L. Reggiani, and L. Varani, *J. Appl. Phys.* 69, 7097 (1991).
39. W. Shockley, J. Copeland, and R. James, in "Quantum Theory of Atoms, Molecules and the Solid State," (P. Lowdin, Ed.), p. 537. Academic Press, New York, 1966.
40. K. M. vanVliet et al., *J. Appl. Phys.* 46, 1804 (1975).
41. K. M. vanVliet et al., *J. Appl. Phys.* 46, 1814 (1975).
42. J. Nougier, J. Vaissiere, D. Gasquet, and A. Motadid, *J. Appl. Phys.* 52, 5683 (1981).
43. K. vanVliet and H. Metha, *Phys. Stat. Sol. B* 106, 11 (1991).
44. J. P. Nougier, *IEEE Trans. Electron Devices* 41, 2034 (1994).
45. P. Shiktorov et. al., *Appl. Phys. Lett.* 71, 3093 (1997).
46. F. Bonani and G. Ghione, *Solid-State Electron.* 43, 285 (1999).
47. P. Shiktorov et al., *Riv. Nuovo Cimento* 24, 1 (2001).
48. N. V. Kampen, "Stochastic Processes in Physics and Chemistry." North-Holland, Amsterdam, 1992.
49. M. Macucci, B. Pellegrini, P. Terreni, and L. Reggiani, *Phys. Stat. Sol. B* 152, 601 (1989).
50. M. Macucci, B. Pellegrini, P. Terreni, and L. Reggiani, *J. Appl. Phys.* 63, 5369 (1988).
51. C. Jacoboni and L. Reggiani, *Rev. Mod. Phys.* 56, 645 (1983).
52. L. Reggiani, P. Lugli, and V. Mitin, *Appl. Phys. Lett.* 51, 925 (1987).
53. L. Reggiani, P. Lugli, and V. Mitin, *Phys. Rev. Lett.* 60, 736 (1988).
54. L. Reggiani, L. Varani, P. Lugli, and V. Mitin, in "Proceedings of the 6th Internat. Nasecode Conf." (J. Miller, Ed.), Boole Press, Dublin, 1989.
55. L. Reggiani, L. Varani, V. Mitin, and C. vanVliet, *Phys. Rev. Lett.* 63, 1094 (1989).
56. L. Reggiani et al., *J. Appl. Phys.* 66, 5404 (1989).
57. T. Kuhn, L. Reggiani, and L. Varani, *Phys. Rev. B* 42, 11133 (1990).
58. L. Reggiani and L. Varani, *Nuovo Cimento D* 13, 647 (1991).
59. L. Reggiani, T. Kuhn, and L. Varani, *Comput. Phys. Comm.* 67, 135 (1991).
60. T. Kuhn et al., *Phys. Rev. B* 44, 1074 (1991).
61. L. Reggiani, T. Kuhn, and L. Varani, *Appl. Phys.* 54, 411 (1992).
62. C. Moglestue, "Monte Carlo Simulation of Semiconductor Devices." Science Publishers/Chapman & Hall, London, 1993.
63. L. Varani, T. Kuhn, L. Reggiani, and C. vanVliet, in "Proceedings of the 11th Internat. Conf. on Noise in Phys. Syst. and $1/f$ Fluct." (M. Y. T. Musha and S. Sato, Eds.), p. 59. Omsha, Tokyo, 1991.
64. L. Varani et al., *Phys. Rev. B* 48, 4405 (1993).
65. J. Vaissiere, Ph.D. Thesis, University of Montpellier II, 1986.
66. J. Vaissiere, in "Noise in Physical Systems and $1/f$ Fluctuations" (C. Clays and E. Simoen, Eds.), p. 130. World Scientific, Singapore, 1997.
67. C. Pennetta, G. Trefan, and L. Reggiani, in "Unsolved Problem on Noise," (L. Kish and D. Abbott, Eds.), American Instutute of Physics, New York, 2000.
68. C. Pennetta, L. Reggiani, and G. Trefan, *Phys. Rev. Lett.* 85, 5238 (2000).
69. M. Rimini-Döring, A. Hangleiter, and N. Klötzer, *Phys. Rev. B* 45, 1163 (1992).
70. A. Longoni, E. Gatti, and R. Sacco, *J. Appl. Phys.* 78, 6283 (1995).
71. A. Godoy, J. Jimenez-Tejada, A. Palma, and P. Cartujo, *J. Appl. Phys.* 82, 3351 (1997).
72. S. Perez, T. Gonzalez, S. Delage, and J. Obregon, *Semicond. Sci. Technol.* 16, L1 (2001).
73. B. Schmithüsen, A. Schenk, and W. Fichtner, Tech. Rep. 00/8, Integrated System Laboratory, 2000.
74. F. Pascal, S. Jarrix, C. Delseny, and J. Lecoy, J. Appl. Phys. 79, 3046 (1996).
75. G. Bosman and J. Zijlstra, *Solid-State Electron.* 25, 273 (1982).
76. L. Lust and J. Kakalios, *Phys. Rev. Lett.* 75, 2192 (1995).
77. A. Rice and K. Malloy, *J. Appl. Phys.* 87, 7802 (2000).
78. N. Paul, C. M. vanVliet, and S. Mergui, *J. Appl. Phys.* 85, 8287 (1999).
79. M. Levinshtein, S. Rumyantsev, J. Palmour, and D. S. Jr., *J. Appl. Phys.* 81, 1758 (1997).
80. L. Chen, C. vanVliet, P. Koenraad, and G. Larkins, *J. Appl. Phys.* 86, 6206 (1999).
81. "Noise in Physical Systems and $1/f$ Fluctuations" (S. S. T. Musha and M. Yamamoto, Eds.), Ohmsha, Tokyo, 1991.
82. "Noise in Physical Systems and $1/f$ Fluctuations" (P. Handel and A. Chung, Eds.), American Institute of Physics, New York, 1993.
83. "Noise in Physical Systems and $1/f$ Fluctuations" (V. Bareikis and R. Katilius, Eds.), World Scientific, Singapore, 1995.
84. "Noise in Physical Systems and $1/f$ Fluctuations" (C. Clays and E. Simoen, Eds.), World Scientific, Singapore, 1997.
85. "Noise in Physical Systems and $1/f$ Fluctuations" (C. Surya, Ed.), Bentham Press, London, 1999.
86. "Noise in Physical Systems and $1/f$ Fluctuations" (G. Bosman, Ed.), World Scientific, Singapore, 2001.
87. S. Jarrix, C. Delseny, F. Pascal, and G. Lecoy, *J. Appl. Phys.* 81, 2651 (1997).
88. C. Delseny, F. Pascal, S. Jarrix, and G. Lecoy, *J. Appl. Phys.* 81, 2658 (1997).
89. V. Shadrin, V. Mitin, K. Choi, and V. Kochelap, *J. Appl. Phys.* 78, 5765 (1995).
90. V. Mitin et al., *Infrared Phys. Technol.* 42, 467 (2000).
91. V. Ryzhii et al., *Appl. Phys. Lett.* 78, 3523 (2001).
92. M. Deen, S. Rumyantsev, R. Bashir, and R. Taylor, *J. Appl. Phys.* 84, 625 (1998).
93. S. Rumyantsev et al., *J. Appl. Phys.* 87, 1849 (2000).
94. S. Machlup, *J. Appl. Phys.* 25, 341 (1954).
95. A. Panarier et al., in "Noise in Physical Systems and $1/f$ Fluctuations" (G. Bisman, Ed.), p. 379. World Scientific, Singapore, 2001.
96. J. Bernamont, *Ann. Phys.* 7, 71 (1937).
97. R. Suris and B. Fuks, *Sov. Phys. Semicond.* 14, 641 (1980).
98. J. Davies, P. Hyldgaard, S. Hershfield, and J. Wilkins, *Phys. Rev. B* 46, 9620 (1992).
99. G. Iannaccone, M. Macucci, and B. Pellegrini, *Phys. Rev. B* 55, 4539 (1997).
100. V. Y. Aleshkin, L. Reggiani, and A. Reklaitis, *Phys. Rev. B* 63, 085302 (2001).